HHS Public Access

Author manuscript

Cell Rep. Author manuscript; available in PMC 2019 February 20.

Published in final edited form as:

Cell Rep. 2019 January 22; 26(4): 893–905.e4. doi:10.1016/j.celrep.2018.12.096.

Evolution of Relapse-Proficient Subclones Constrained by Collateral Sensitivity to Oncogene Overdose in Wnt-Driven Mammary Cancer

Ross R. Keller[1,2,4] and **Edward J. Gunther**[1,2,3,5,*]

[1]Jake Gittlen Cancer Research Foundation, Pennsylvania State University College of Medicine, Hershey, PA 17033, USA

[2]Penn State Hershey Cancer Institute, Pennsylvania State University College of Medicine, Hershey, PA 17033, USA

[3]Department of Medicine, Pennsylvania State University College of Medicine, Hershey, PA 17033, USA

[5]Lead Contact

SUMMARY

Targeted cancer therapeutics select for drug-resistant rescue subclones (RSCs), which typically carry rescue mutations that restore oncogenic signaling. Whereas mutations underlying antibiotic resistance frequently burden drug-naive microbes with a fitness cost, it remains unknown whether and how rescue mutations underlying cancer relapse encounter negative selection prior to targeted therapy. Here, using mouse models of reversible, Wnt-driven mam-mary cancer, we uncovered stringent counter-selection against Wnt signaling overdose during the clonal evolution of RSCs. Analyzing recurrent tumors emerging during simulated targeted therapy (Wnt withdrawal) by multi-region DNA sequencing revealed polyclonal relapses comprised of multiple RSCs, which bear distinct but functionally equivalent rescue mutations that converge on sub-maximal Wnt pathway activation. When superimposed on native (i.e., undrugged) signaling, these rescue mutations faced negative selection, indicating that they burden RSCs with a fitness cost before Wnt withdrawal unmasks their selective advantage. Exploiting collateral sensitivity to oncogene overdose may help eliminate RSCs and prevent cancer relapse.

Graphical Abstract

*Correspondence: ejg12@psu.edu.

[4]Present address: Memorial Sloan Kettering Cancer Center, New York, NY 10065, USA

AUTHOR CONTRIBUTIONS

Conceptualization, R.R.K. and E.J.G.; Methodology, R.R.K. and E.J.G.; Investigation, R.R.K.; Writing – Original Draft, R.R.K. and E.J.G.; Writing – Review and Editing, R.R.K. and E.J.G.; Visualization, R.R.K. and E.J.G.; Funding Acquisition, E.J.G.

SUPPLEMENTAL INFORMATION

Supplemental Information includes seven figures and can be found with this article online at https://doi.org/10.1016/j.celrep.2018.12.096.

DECLARATION OF INTERESTS

The authors declare no competing interests.

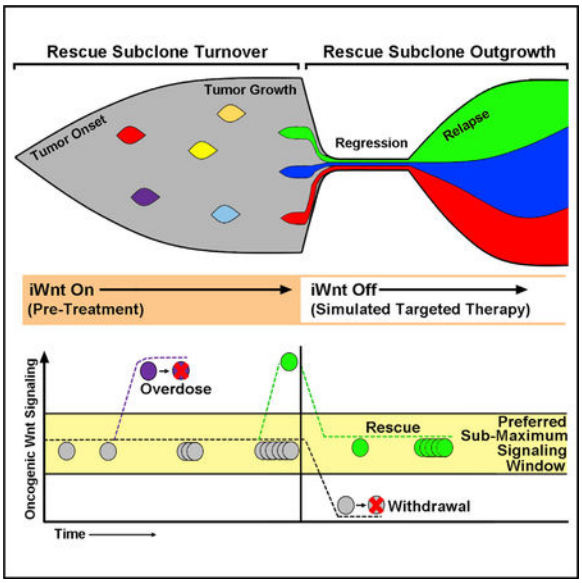

In Brief

Keller and Gunther show that Wnt-driven mammary cancers challenged with simulated targeted therapy (Wnt withdrawal) undergo clonal evolution, which stringently selects for mutations that restore a “just right” level of oncogenic signaling. Therefore, cancer relapses emerge from rare subclones that are encumbered by an untapped vulnerability to oncogene overdose.

INTRODUCTION

Even when targeted therapy results in cancer remission, relapse can emerge from rare drug-resistant cells (Bozic et al., 2013; Hughes and Andersson, 2015; McGranahan and Swanton, 2017). Indeed, mathematical modeling predicts that clinically detectable, treatment-naive cancers nearly always harbor one or more rescue subclones (RSCs) equipped to seed relapse (Bozic et al., 2013; Diaz et al., 2012). In practice, RSC populations can be vanishingly small, precluding routine RSC detection within clinical specimens until relapse is well underway. Moreover, the detection and enumeration of unique RSCs at relapse can be confounded by parallel evolution. For example, because RSCs typically are identified by their rescue mutations, RSCs falsely appear clonally related when they independently acquire identical, highly recurrent rescue mutations. As such, how evolutionary pressures act in the pre-treatment setting to influence the number, size, and turnover of discrete RSC populations remains obscure.

Targeted therapies typically exploit a phenomenon termed oncogene addiction, wherein cancer cells show exquisite dependence on an aberrantly activated signaling pathway for survival and/or proliferation (Weinstein, 2002). Inversely, diverse basic and clinical research findings indicate that cancer cells become impaired not only when challenged by oncogene withdrawal but also when confronted by oncogene overdose. Over-expressing potent oncogenes in untransformed cells paradoxically triggers proliferation arrest or cell death in cell culture and in mouse models (Nieto et al., 2017; Sarkisian et al., 2007; Serrano et al.,

1997). Similarly, certain cancers almost never acquire two driver mutations that potently activate the same oncogenic signaling pathway, perhaps because concerted action of strong activating events triggers overdose (Ambrogio et al., 2017; Unni et al., 2015). In the clinic, sensitivity to excessive oncogenic signaling likely explains why pharmacologic doses of gonadal hormones paradoxically served as effective treatment for hormone-dependent breast cancers before the advent of modern anti-hormonal drugs (Haddow et al., 1944; Jordan and Ford, 2011). More recently, oncogene overdose has been invoked to explain why some cancers, after adapting to potent targeted therapy, paradoxically depend upon continued drug treatment for maintenance and growth (Amin et al., 2015a, 2015b; Das Thakur et al., 2013; Sun et al., 2014). Intriguingly, preclinical models of melanoma, lymphoma, and prostate cancer have led to clinical trials aimed at exploiting oncogene overdose for therapeutic gain in patients (Amin et al., 2015a; Schweizer et al., 2015). Despite these advances, it remains unclear whether and how oncogene overdose shapes the evolution of incipient RSCs prior to treatment.

To model targeted therapy of breast cancer, we previously engineered mice for reversible activation of oncogenic Wnt signaling. In female inducible Wnt1 (iWnt) mice, doxycycline (Dox)-induced expression of a *Wnt1* transgene leads to the stochastic onset of Wnt-driven mammary carcinomas. iWnt tumors regress upon simulated targeted therapy (withdrawal of inducer-dependent Wnt1 expression) and then relapse later with rescue mutations that restore Wnt signaling (Debies et al., 2008; Gunther et al., 2003). Most iWnt relapses acquire one of two rescue mutations: either an activating mutation in the downstream Wnt transducer β-catenin (encoded by *Ctnnb1*; hereafter b-*Cat*) or a mutation corrupting the *rtTA* gene switch (enabling Dox-independent expression of the *Wnt1* transgene; Cleary et al., 2014). These rescue mutations are highly recurrent, which limits detection of discrete RSCs. When reconstructing the clonal evolution of human cancers, mapping distinct, functionally equivalent tumor suppressor gene mutations to spatially separated tumor sites can reveal discrete subclones evolving in parallel (Gerlinger et al., 2012; Juric et al., 2015). To render clonal evolution in the iWnt model more amenable to genetic analysis, we introduced a germline Apc^{Min} allele (Moser et al., 1993), thereby inactivating one copy of the *Adenomatous polyposis coli* (*Apc*) tumor suppressor gene that normally restrains Wnt signaling.

We reasoned that iWnt/$Apc^{Min/+}$ tumors should be sensitized to relapse via somatic, inactivating second-hit *Apc* mutations, which might inform on RSC evolution in two key ways. First, selection for *Apc* second hits ought to broaden the range of functionally equivalent rescue mutations with which to distinguish independent RSCs. Second, the precise location of second-hit *Apc* mutations ought to provide a crucial readout of the level of Wnt signaling favored at relapse. In human colorectal cancers, second-hit *APC* mutations are contingent upon the first *APC* hit (whether inherited or sporadic) in a manner that selects for maintaining some residual APC-mediated restraint on Wnt signaling (Albuquerque et al., 2002; Rowan et al., 2000). Similarly, studies employing either allelic series of targeted *Apc* mutations or inducible Apc knockdown in mice consistently show that genotypes conferring graded reductions in *Apc* function specify graded increases in Wnt signaling (Buchert et al., 2010; Dow et al., 2015; Kielman et al., 2002; Premsrirut et al., 2011). Most notably, hypomorphic mutations that create premature stop codons in the *Apc* mammary tumor

mutation cluster region (*Apc*^{mmcr}; ranging from *Apc* codons 1,512–1,580; Figure 1A), when paired with a near null *Apc* allele (e.g., *Apc*^{Min}), specify a sub-maximum level of Wnt pathway activation that is uniquely suited to initiating mammary carcinogenesis (Bakker et al., 2013; Gaspar et al., 2009; Kuraguchi et al., 2009; Toki et al., 2013). Whether such cancers, once established, are constrained to maintain sub-maximum Wnt signaling during tumor progression remains unknown.

RESULTS

Relapse after Wnt Withdrawal Selects for Hypomorphic Apc Mutations and Sub-maximum Wnt Signaling

To test whether a germline *Apc*^{Min} allele promotes relapse, primary mammary tumors arising on iWnt/*Apc*$^{Min/+}$ and iWnt/*Apc*$^{+/+}$ mice were explanted onto wild-type, syngeneic hosts. Thereafter, mice bearing established outgrowths were subjected to Wnt withdrawal and monitored through regression and relapse. As expected, relapses arose more quickly from iWnt/*Apc*$^{Min/+}$ tumor explants than from their iWnt/*Apc*$^{+/+}$ counterparts (Figure 1B). Sequencing of *Apc* alleles from iWnt/*Apc*$^{Min/+}$ tumor biopsy samples collected prior to Wnt withdrawal failed to uncover *Apc*^{mmcr} mutations or loss-of-heterozygosity (LOH) events, consistent with negligible selection against *Apc* function in this context (0 of 14 tumor biopsies; 0%). However, relapses arising after Wnt withdrawal nearly always acquired a hypomorphic, second-hit *Apc*^{mmcr} nonsense mutation (31 of 34 tumors; 94%; Figure 1C). Underscoring selective pressure favoring acquisition of a specific hypomorphic allele, these *Apc*^{mmcr} mutations co-localized within a 200-bp gene segment that comprises only 2.4% of the *Apc* coding region. Moreover, these relapses rarely underwent *Apc* LOH (i.e., somatic loss of the germline *Apc*$^{wild\text{-}type}$ allele; only 1 of 24 tumors; 4%; Figure S1A), indicating stringent selection for an *Apc*$^{Min/mmcr}$ tumor cell geno-type. By contrast, *Apc*$^{Min/+}$ intestinal adenomas routinely underwent LOH as previously described (Haigis and Dove, 2003), consistent with selection for complete loss of the Apc-mediated restraint on Wnt signaling in intestinal tumor cells (Figure S1B). *Wnt1* transgene expression, which was robust in primary iWnt/*Apc*$^{Min/+}$ mammary tumors, dropped to nearly undetectable levels at relapse, suggesting second-hit *Apc*^{mmcr} rescue mutations are sufficient for Wnt pathway reactivation (Figure 1D).

Next, we tested whether rescue mutations generating an *Apc*$^{Min/mmcr}$ tumor cell genotype confer sub-maximum Wnt pathway activation by performing β-cat immunohistochemistry on tissue and tumor sections. Stabilization of β-cat culminates in cytosolic accumulation and nuclear translocation, which serve as classic hallmarks of activated Wnt signaling. In the intestine, weak, membrane-associated β-cat expression in normal epithelium contrasted with strong nuclear-localized expression in adenomas, as others have described (Figure S2). In both normal mammary gland and tumors arising in the MMTV-*Myc* transgenic mouse model (Stewart et al., 1984), only weak membrane-associated β-cat was detected, consistent with negligible Wnt pathway activation (Figure 1E). By comparison, mammary tumors from iWnt/*Apc*$^{Min/+}$ mice consistently stained more strongly for b-cat, with evidence for modest cytosolic accumulation as well as weak nuclear-localized staining in some cells. Notably, despite the cell-to-cell variability evident within each tissue section, the overall level and

pattern of β-cat expression was remarkably conserved across primary and relapsed mammary tumors, suggesting selection for a preferred Wnt pathway activation level. Confirming that this preferred signaling level resides below that which is conferred by complete *Apc* loss of function, the lone mammary tumor relapse in our set that underwent *Apc* LOH showed strong, nuclear-localized β-cat expression on par with that observed in intestinal adenomas (Figures 1E and S2). Why this relapse was unique in evading selection for the recurring $Apc^{Min/mmcr}$ tumor cell genotype is unclear. Nonetheless, in sum, our findings underscore strong selection for a sub-maximum Wnt signaling window during mammary tumorigenesis, as others have proposed. Extending this concept, we find that selection for this signaling window is conserved across diverse Wnt pathway-driven mammary tumor models, because relapses arising in iWnt/$Apc^{Min/+}$ mice resemble primary mammary tumors arising in carcinogen-exposed $Apc^{Min/+}$ mice (Keller et al., 2016) by converging on the same $Apc^{Min/mmcr}$ tumor cell genotype. Moreover, our modeling shows that the constraint to maintain sub-maximum Wnt signaling persists during later stages of tumor progression, because invasive tumor explants maintain selection for the $Apc^{Min/mmcr}$ tumor cell genotype, even as they undergo clonal evolution to spawn relapse.

Polyclonal Relapse and Turnover of RSCs during Serial Passage of Wnt-Driven Tumors

In pilot studies, we often detected two distinct Apc^{mmcr} nonsense mutations in a single relapse sample, suggesting some iWnt/$Apc^{Min/+}$ relapses may derive from multiple distinct RSCs. To assess polyclonality in depth, we adopted a multi-region sequencing (MRS) protocol in which relapses routinely were divided into 18 segments prior to targeted re-sequencing of *Apc* alleles (Figure 2). Mapping Apc^{mmcr} mutations onto tumor segments revealed that most iWnt/$Apc^{Min/+}$ relapses harbored multiple distinct RSCs, which typically occupied contiguous, non-overlapping territories. Even in polyclonal relapses, each individual tumor segment usually harbored a single predominant Apc^{mmcr} rescue mutation detectable by Sanger sequencing, suggesting that RSC outgrowth following Wnt withdrawal primarily involves local clone expansion, with relatively little clone intermingling via local micro-invasion or tumor self-seeding (Figure 2). To enable more sensitive detection of low-prevalence mutant alleles, representative relapse segments underwent further analysis of the Apc^{mmcr} region by high-throughput re-sequencing (hereafter, HTS) on the Illumina platform. Again, most segments derived from polyclonal relapses harbored a single predominant Apc^{mmcr} rescue mutation, indicating that polyclonal relapses tended to be conglomerates of macroscopic, primarily monoclonal RSCs (Figure S3). However, we cannot rule out the possibility that low-prevalence RSCs lacking Apc^{mmcr} mutations sometimes contribute as admixed subclones.

To determine whether RSCs derive from stable subpopulations of tumor cells lurking within primary tumor explants prior to Wnt withdrawal, RSC maps were generated for a set of relapses arising within two independent iWnt/$Apc^{Min/+}$ tumor lineages, each propagated through multiple generations of serial passage on Dox-treated hosts (Figure 3A). For each lineage analyzed, the number of RSCs per relapse detected after Wnt withdrawal remained stable through serial passage, arguing for little or no accumulation of RSCs over time. Concordantly, for the first tumor lineage (hereafter lineage A), nearly all of the RSC-defining Apc^{mmcr} rescue mutations identified across passage generations were unique (18 of

20; 90%), indicating that RSCs likely arose *de novo* during tumor outgrowth at each generation and were not propagated host to host during tumor passage (Figure 3B, left panels). Incidentally, we noted multiple gross lung lesions at necropsy in three mice bearing iWnt/Apc$^{Min/+}$relapses from lineage A. In each case, all distant lung lesions carried an *Apc*^{mmcr} somatic mutation matching a single clone within the local relapse, indicating monophyletic spread of metastases during relapse (Figures 3B and S3). Analysis of a second independent tumor lineage (hereafter lineage B) likewise failed to reveal pervasive, long-lived RSCs (Figure 3B, right panels). Again, most rescue mutations identified in lineage B were unique (17 of 25; 68%), and novel rescue mutations continued to appear in late-passage tumors. Moreover, comparing rescue mutations across explant generations showed that a subset of mutations that recurred went absent from one or more intervening passages, suggesting they likely arose independently (Figure 3B).

Compared with explants from lineage A, explants from lineage B on average showed reduced relapse-free survival following Wnt withdrawal as well as increased polyclonality at relapse (i.e., more RSCs per relapse) detected by MRS analysis (Figure 3C). The mechanism(s) underlying these differences remain unknown but presumably stem from traits acquired during the clonal evolution of each ancestral primary tumor. In any event, the distinct behavior of these lineages offers an intriguing link between increased polyclonality and more rapid onset of tumor escape.

Rapid Turnover of RSCs Generated by Mutagen Exposure

Next, we devised a strategy for detecting turnover of RSCs during growth of iWnt/*Apc*$^{Min/+}$ tumors. When exploring the range of rescue mutations capable of subverting targeted therapy, researchers often employ accelerated mutagenesis protocols, wherein treatment of a drug-sensitive tumor cell population is preceded by exposure to a potent mutagen. Although mutations are introduced genome-wide, subsequent drug treatment strongly selects for rescue mutations that drive RSC outgrowth (Brammeld et al., 2017). If RSCs are short lived prior to targeted therapy, we reasoned that the number of RSCs available to seed relapse ought to rise in the immediate aftermath of a mutagen exposure capable of generating rescue mutations and then quickly decline due to RSC turnover. To test this model prospectively, mice bearing sibling, iWnt/*Apc*$^{Min/+}$ tumor explants either remained unexposed (mutagen-naive throughout Wnt withdrawal and relapse) or received a one-time dose of a fast-acting chemical mutagen, *N*-ethyl-*N*-nitrosourea (ENU), either two days or seven days prior to Wnt withdrawal (Figure 4A).

Compared with unexposed control tumors, ENU exposure 2 days before Wnt withdrawal (day$_{-2}$ ENU) dramatically has tened relapse onset and increased the number of RSCs per relapse detected via MRS, as expected (Figure 4B). Indeed, the number of RSCs arising after day$_{-2}$ ENU exceeded the number of tumor segments analyzed, meaning that individual tumor segments themselves typically were polyclonal (Figure S4). Paradoxically, highly polyclonal tumor segments comprised of multiple *Apc*^{mmcr} mutant RSCs appeared wild-type when initially assessed by Sanger sequencing, because this low-sensitivity technique only detects an allelic variant that reaches a minimum prevalence of about 10%–15%, which corresponds to an RSC that reaches a minimum prevalence of 20%–30% of the cells

analyzed (assuming *Apc*^{mmcr} mutations are heterozygous and unperturbed by copy number variation). By contrast, analyzing *Apc*^{mmcr} alleles by HTS permitted detection of mutant alleles above a threshold of about 0.3% prevalence, which enabled detection of as many as 9 distinct, low-prevalence *Apc*^{mmcr} mutant RSCs residing in a single relapse segment (Figure S4). We confirmed that these day$_{-2}$ ENU relapse segments were indeed highly polyclonal by two additional means. In one strategy, relapse segments, which typically measured 3–5 mm in diameter, were first subdivided into sub-millimeter fragments before preparing genomic DNA (gDNA) templates for analysis. Subsequent Sanger sequencing of PCR-amplified *Apc*^{mmcr} alleles detected multiple rescue mutations distributed among the subdivided tumor fragments (Figure S5). In a second strategy, bulk gDNA templates from putative polyclonal segments were used to generate PCR-amplified *Apc*^{mmcr} alleles as before, but alleles were subcloned prior to Sanger sequencing. Again, rescue mutations that eluded detection on bulk analysis were detected readily after subcloning (Figure S5), indicating these day$_{-2}$ ENU tumor segments are indeed composites of numerous minute RSCs. Remarkably, moving ENU exposure from day$_{-2}$ to day$_{-7}$ significantly reduced ENU's impact on both relapse-free survival and RSCs per relapse, consistent with rapid dropout of short-lived, ENU-initiated RSCs during the added days preceding Wnt withdrawal (Figure 4B).

In a parallel arm of this experiment, an additional set of tumors was subjected to an interrupted Wnt withdrawal schedule to simulate a drug-free break in the midst of targeted therapy (Figure 4A). Here, after day$_{-7}$ ENU exposure, Wnt withdrawal was maintained during two weeks of tumor regression and then transiently reversed until tumors regrew to their original size, whereupon Wnt withdrawal was reinstated for the remainder of the experiment. Interrupted Wnt withdrawal yielded a trend toward prolonged relapse-free survival and generated significantly fewer RSCs per relapse (Figure 4B), consistent with RSC dropout resuming during Wnt pathway reactivation and tumor re-growth.

Examination of *Apc*^{mmcr} mutation spectra confirmed that ENU exposure seeded relapse by generating second-hit *Apc* rescue mutations. Unexposed relapses yielded a mutation spectrum dominated by indels and single nucleotide variants (SNVs) at G:C base pairs, mirroring the spectrum of spontaneous, somatic *Apc*^{mmcr} mutations described previously (Kuraguchi et al., 2009). By contrast, ENU exposure shifted the spectrum away from indels toward SNVs at A:T base pairs (Figure 4C), matching known ENU mutation patterns (Jansen et al., 1994b; Keller et al., 2016). Concordantly, replacing ENU with the related mutagen *N*-methyl-*N*-nitrosourea (MNU) similarly hastened relapse and increased RSCs per relapse while generating a distinct, MNU-specific mutation spectrum (Figures 4B and4C). Notably, despite MNU's known propensity to induce G:C to A:T base substitutions (Jansen et al., 1994a; Westcott et al., 2015), sense-strand G > A SNVs were completely absent from our *Apc*^{mmcr}-derived mutation spectrum, reflecting a genetic coding constraint. Specifically, the *Apc*^{mmcr} lacks a TGG codon, the only codon capable of converting to a stop codon via a G > A SNV. We hypothesized that this coding constraint, coupled with the constraint to restore sub-maximum Wnt signaling, might channel sense-strand G > A SNVs toward rescue mutations in alternative target genes. Indeed, whereas ENU-exposed relapses harbored an *Apc*^{mmcr} rescue mutation in nearly every tumor segment (Figure S5), fully one-third of MNU-exposed relapse segments lacked an *Apc*^{mmcr} mutation (35 of 105; 33%), and

a subset of these segments instead harbored β-cat or *rtTA* rescue mutations, which invariably were sense-strand G > A SNVs (Figure 4D).

Relapses Converge on Sub-maximum Wnt Reactivation in the Absence of a Sensitizing *Apc*^{Min} Mutation

Surprisingly, acquisition of *Apc*^{mmcr} rescue mutations did not strictly require a sensitizing germline *Apc*^{Min} mutation. Whereas mutagen-naive iWnt/*Apc*$^{+/+}$ tumors were slow to relapse and acquired dominantly acting β-cat rescue mutations in line with our previous work, ENU-exposed iWnt/*Apc*$^{+/+}$ tumors relapsed quickly and invariably acquired *Apc*^{mmcr} rescue mutations instead of β-cat mutations (Figures 5A and5B), as did a subset of MNU-exposed tumors (see below). Because a single intact *Apc* allele normally suffices to restrain Wnt signaling, we searched for collaborating second-hit *Apc* mutations. Remarkably, these *Apc*^{mmcr} mutant relapses nearly always carried a second somatic inactivating mutation further upstream in *Apc* (15 of 16 tumors; 94%; Figure 5C). We refer to these somatic upstream *Apc* mutations as "*Min-like*," because they encode truncated proteins similarly devoid of all (or nearly all) of the seven 20-amino-acid repeats implicated in β-catenin downregulation. Several observations suggest that mutagen exposure may generate biallelic *Apc* inactivation through a complex mutational process involving quasi-synchronous *Apc* hits, rather than sequential, metachronous *Apc* hits. First, neither *Apc* hit on its own is expected to provide a sizable selective advantage that drives clonal expansion, making sequential acquisition of *Apc* hits statistically unlikely. Second, four relapses were found to be comprised of two distinct RSCs, each carrying a unique *Apc*$^{Min\text{-}like/mmcr}$ genotype. Subclone maps from these relapses showed that neighboring tumor segments never shared one *Apc* hit, but not the other, as might be expected to occur if hits accrued metachronously (Figure S6A). Third, when the mutations that generated *Apc*^{mmcr} versus *Apc*$^{Min\text{-}like}$ alleles were analyzed separately, both mutation sets yielded spectra attribut able to ENU exposure, despite ENU's short-lived mutagenic activity *in vivo* (Probst and Justice, 2010; Figure S6B). In any case, stringent selection for sub-maximum Wnt signaling yielded a recurring *Apc*$^{Min\text{-}like/mmcr}$ tumor cell genotype in mutagen-exposed iWnt/*Apc*$^{+/+}$ relapses, recapitulating the recurring *Apc*$^{Min/mmcr}$ genotype encountered in sensitized iWnt/Apc$^{Min/+}$ relapses. Crucially, these relapses converge on *Apc* allele pairs that, in sum, retain 3 or 4 β-catenin degradation domains (Figure 5C), again indicating robust selection for a preferred Wnt signaling level conducive to mammary tumor maintenance (Bakker et al., 2013). Concordantly, relapses that acquired biallelic mutations culminating in the *Apc*$^{Min\text{-}like/mmcr}$ tumor cell genotype showed sub-maximum β-cat immunostaining on par with their antecedent primary tumors (Figure S2).

Whereas MNU-exposed iWnt/*Apc*$^{+/+}$ tumors relapsed even faster than their ENU-exposed counterparts (Figure 5A), they only rarely relapsed with biallelic *Apc* rescue mutations (3 of 15 tumors; 20%), likely due to the coding constraints discussed above that disfavor acquisition of MNU-induced nonsense mutations within the *Apc*^{mmcr}. Instead, MNU-exposed relapses often acquired β-cat or *rtTA* rescue mutations (Figure 5B), which invariably were sense-strand G > A SNVs, as before (Figure 5D). Together, these findings underscore how exposure-specific mutation spectra, when filtered through narrow signaling

requirements and coding constraints, can bias rescue mutations toward “preferred” driver genes with remarkable specificity (Keller et al., 2016).

Negative Selection of RSCs under Conditions Predicted to Drive Wnt Signaling Overdose

Returning to iWnt/$Apc^{Min/+}$ tumors, we considered whether the rapid dropout of mutagen-initiated RSCs prior to Wnt withdrawal might occur by neutral drift rather than by counter-selection against Wnt signaling overdose. To test whether parental tumor cells compete neutrally with RSC cells, we compared their relative clonal expansion in a competitive tumor reconstitution assay. Single-cell suspensions were prepared concurrently from three freshly harvested, sibling iWnt/$Apc^{Min/+}$ tumor specimens (schematized in Figure 6). P cells (denoting parental) were prepared from a Wnt-dependent primary tumor explant. R1 and R2 cells (denoting relapse) were prepared from distinct segments of a putative polyclonal relapse, which arose from a sibling explant during Wnt withdrawal. R1 and R2 cells were generated from antipodal segments to maximize the likelihood of sampling distinct RSC populations. Then tumors were reconstituted in the mammary fat pads of syngeneic, Dox-treated host mice by injecting each cell population individually (P-only, R1-only, and R2-only control injections) or by co-injecting admixed populations. Specifically, R2 cells were competed against both R1 cells (R1 + R2 injections) and P cells (P + R2 injections). Due to limiting tumor cell numbers, we did not compete R1 cells against P cells (i.e., P + R1 injections were not performed). Injections of all individual and admixed tumor cell populations yielded tumors that arose promptly and grew synchronously, permitting all necropsies and tumor harvests to be performed on the same day. Finally, MRS was performed on each reconstituted tumor to assess the contribution of individual subclones.

P-only injection yielded tumor segments lacking detectable Apc^{mmcr} mutations, as expected. By contrast, R1-only injection yielded a monoclonal tumor bearing an $Apc^{1540C > T}$ mutation in all segments. Interestingly, R2-only injection yielded a tumor comprised of both Apc^{1568+T} and $Apc^{1522A > T}$ mutant segments, indicating R2 cells (unbeknownst to us at the time of injection) derived from a polyclonal tumor segment (Figure 6). Consistent with neutral competition among the distinct RSCs, R1 + R2 co-injections yielded polyclonal tumors comprised of all three component RSCs, and the contribution from each RSC matched well with its relative population size at injection (see STAR Methods). By contrast, in P + R2 co-injections, R2-derived RSC cells contributed little to tumor reconstitution, consistent with parental cells outcompeting RSCs (Figure 6).

We also sought direct evidence for oncogene overdose-mediated clone dropout in a prospective lineage tracing experiment. Previously, we showed that ENU-initiated primary mammary tumors arising in Apc^{Min} mice invariably carry second-hit Apc^{mmcr} mutations, yielding an $Apc^{Min/mmcr}$ tumor cell genotype (Keller et al., 2016). We reasoned that converting hypomorphic Apc^{mmcr} to a null allele ought to abolish the residual Apc^{mmcr}-mediated restraint on Wnt signaling, triggering oncogene overdose and clone dropout in mammary tumor cells, but not intestinal tumor cells (which routinely undergo LOH to create an $Apc^{Min/Min}$ tumor cell genotype; Haigis and Dove, 2003). To test this model, first we modified Apc^{Min} mice by introducing transgenes that enable tamoxifen (Tam)-inducible, Cre-mediated multi-color lineage tracing (UBC-Cre^{ERT} and R26R-*Confetti*; hereafter

Confetti; Figure S7A; Ruzankina et al., 2007; Snippert et al., 2010). Next, for comparison against $Apc^{Min/+}$/Confetti control mice, we generated experimental mice that additionally carry a conditional knockout allele of *Apc* (hereafter Apc^{CKO}; Kuraguchi et al., 2006). In summary, as schematized in Figure 7A, Tam treatment initiates lineage tracing in both $Apc^{Min/+}$/Confetti control mice and $Apc^{Min/CKO}$/Confetti experimental mice. However, only experimental mice undergo Cre-mediated recombination at the *Apc* locus, thereby converting the Apc^{CKO} allele (which functionally approximates wild-type *Apc*) to $Apc^{\Delta 580}$ (which functionally approximates near null Apc^{Min}; Kuraguchi et al., 2006).

After confirming that the *Confetti* transgene combination permits Tam-inducible lineage tracing in mammary epithelium (Figure S7), we generated ENU-initiated mammary tumors in both $Apc^{Min/CKO}$/*Confetti* experimental mice and $Apc^{Min/+}$/*Confetti* controls. Because of the stringent selection for Apc^{mmcr} second-hit mutations, control mammary tumors acquired a “Cre-indifferent” $Apc^{Min/mmcr}$ tumor cell genotype, whereas experimental mammary tumors acquired a “Cre-modifiable” $Apc^{Min/CKO\text{-}mmcr}$ tumor cell genotype, which can convert to $Apc^{Min/\Delta 580}$ upon recombination (Figure 7A). Tumor-bearing mice then were dosed with Tam to initiate tracing of both mam-mary and intestinal tumor cell clones while simultaneously inactivating the Apc^{CKO} allele. In control mice, clones residing in both mammary tumors and intestinal tumors at day 2 of the trace comprised mostly solitary labeled cells, which typically expanded to monochrome cell clusters at day 7, as expected. In experimental mice, tracing of intestinal tumor clones was un-perturbed by the Apc^{CKO} allele, but tracing of mammary tumor clones showed a marked reduction in labeled cells at day 2 and a near absence of labeled cells at day 7, indicating dropout of mammary, but not intestinal, tumor cell clones (Figures 7B and7C). Concordantly, recombined Apc^{CKO} alleles were detectable in these mammary tumors using a PCR-based assay (Kuraguchi et al., 2006) at day 2, but not at day 7 (Figures S7D and S7E). Thus, dropout of recombined tumor cells was highly context dependent, consistent with the lower Wnt signaling level window conducive to mammary versus intestinal tumor growth. Together, our clone competition and lineage-tracing studies strongly reinforce the causal link between oncogene overdose and clone dropout.

DISCUSSION

Potent targeted therapy triggers regression of oncogene-addicted cancers, but most patients relapse within months due to selection for rare tumor cells, which frequently carry rescue mutations that restore oncogenic signaling. Although rescue mutations often pre-exist drug treatment (Bhang et al., 2015; Diaz et al., 2012; Hata et al., 2016; Misale et al., 2012; Turke et al., 2010), the evolutionary dynamics shaping drug-resistant RSC populations prior to targeted therapy remain obscure. Here, by mapping the clonal evolution of relapse in mouse models of breast cancer, we show that rescue mutations can impose collateral sensitivity to oncogene overdose, thereby driving potent negative selection prior to oncogene withdrawal. To make this observation, we developed mouse modeling strategies that enabled the detection of dozens of distinct, yet functionally equivalent, Apc^{mmcr} rescue mutations, which unequivocally subvert Wnt withdrawal by acting as drivers of mammary cancer relapse. Notably, we defined experimental conditions in which simulated targeted therapy reliably culminates in polyclonal relapse, creating opportunities to model a commonly

encountered clinical scenario (Burrell and Swanton, 2014). Our overall methodology offers an alternative to performing tumor cell lineage tracing using barcoded retroviruses. Although barcoding offers a powerful means of monitoring subclonal lineages as they expand and contract through time (Bhang et al., 2015; Hata et al., 2016), the tracing experiments are conducted using cell culture, and they require *ex vivo* labeling that may be inefficient and biased toward readily transduced subsets of tumor cells (Bystrykh and Belderbos, 2016).

Our analysis of the evolutionary dynamics underlying tumor growth suggests Wnt-driven mammary cancers may be useful for preclinical modeling of adaptive therapy. Whereas traditional cancer treatment protocols are designed to maximize tumor cell killing, adaptive therapy protocols are tailored to forestall tumor growth by exploiting sustained competition between treatment-sensitive and treatment-resistant tumor cell populations (Gate-nby et al., 2009). The concept has shown promise in both preclinical breast cancer models (Enriquez-Navas et al., 2016) and a small-scale clinical trial for prostate cancer (Zhang et al., 2017). Notably, adaptive therapy hinges on rescue mutations imposing a fitness cost during breaks in treatment. Wnt-dependent mammary cancers meet this requirement, because treatment-sensitive parental tumor cells consistently outcompeted treatment-resistant RSCs when simulated targeted therapy was withheld in both tumor reconstitution assays (Figure 6) and *in situ* lineage-tracing studies (Figure 7). Intriguingly, we saw preliminary evidence that simulating a “treatment holiday” in the midst of Wnt withdrawal offers clinical benefit. Compared with continuous Wnt withdrawal, interrupted Wnt withdrawal led to RSC dropout and a trend toward prolonged relapse-free survival (Figures 4A and4B). Although the clinical benefit of this interrupted Wnt withdrawal protocol was modest, it should be noted that we applied it against cancers with elevated RSC burden (owing to prior ENU exposure) and tested only a single treatment break, arbitrarily scheduled to last two weeks. Future studies will test whether more durable control of Wnt-driven mammary cancers can be achieved by incorporating multiple treatment breaks, scheduled with evolutionary principles in mind. Our modeling approach ought to permit changes in RSC prevalence to be quantified during response to different adaptive therapy schedules. Monitoring competing tumor subsets through time may reveal strategies for directing clonal evolution along preferred trajectories that most effectively eradicate RSCs and/or block disease progression.

Our study illustrates how targeted therapy, by imposing precise selective pressure, can favor rescue mutations affecting a narrow range of genes, thereby rendering the evolutionary path to relapse predictable. That said, we found that subtle changes in exposure history led to dramatic shifts favoring rescue mutations in specific genes. In our accelerated mutagenesis studies, rescue mutations were induced by two mutagens, ENU and MNU, which bear striking structural similarity yet generate distinct patterns of DNA base substitutions (Jansen et al., 1994a, 1994b). When overlaid on genetic coding constraints, these mutagen-specific mutation patterns channeled rescue mutations to “preferred” driver genes with remarkable specificity (Figures 4D and5B). These findings underscore how a cancer’s own exposure history can inform efforts to predict the most favored genetic routes to relapse (Keller et al., 2016). Our modeling sets the stage for dissecting mechanisms whereby clinically important mutagenic exposures, such as prior treatments with radiation or chemotherapy, dictate which rescue mutations emerge during subsequent targeted therapy.

Future work will address which cellular mechanism(s) act downstream of Wnt signaling overdose to limit outgrowth of RSCs. Previous studies have implicated either cell death pathways (Kong et al., 2017; Unni et al., 2015; Varmus et al., 2016) or proliferation arrest pathways (Das Thakur et al., 2013; Nieto et al., 2017; Sun et al., 2014) in restricting outgrowth of sub-clones challenged by oncogene overdose. Which cellular mechanisms come into play may vary depending on the tumor type examined and/or which tumor suppressor mechanisms have remained intact during tumor progression.

Our study has several important limitations that preclude direct translation to clinical settings. Because all of our observations derive from mouse models, species differences must be considered when extrapolating our findings to human cancers. In addition, it is worth noting that mutations activating the Wnt pathway have been observed only rarely in human breast cancer (Nik-Zainal et al., 2016). Furthermore, we relied on a genetic simulation of targeted therapy, because clinically useful Wnt pathway inhibitor drugs remain under development. That said, by focusing on the Wnt pathway, we conducted our experiments in a uniquely detailed genetic framework, permitting mechanistic insights into the role of oncogene overdose in clonal evolution. Some of these insights are worth considering in the context of human cancer. For example, selection against overdose in treatment-naive cancers may help to explain why rescue mutations often reside within low-prevalence subclones prior to targeted therapy and why rescue subclone prevalence can drop during breaks in treatment (Siravegna et al., 2015). In addition, our modeling predicts that some highly recurrent rescue mutations observed in the clinic may be common precisely because they elevate oncogenic signaling only modestly in the pre-treatment setting, thereby evading oncogene overdose. Whether clinically important rescue mutations likewise sensitize human cancer cells to oncogene overdose remains to be determined. If so, treatment strategies designed to exploit this vulnerability may help eliminate cancer subclones capable of seeding drug-resistant relapse.

STAR★METHODS

CONTACT FOR REAGENT AND RESOURCE SHARING

Further information and requests for resources and reagents should be directed and will be fulfilled by the Lead Contact, Edward Gunther (ejg12@psu.edu).

EXPERIMENTAL MODEL AND SUBJECT DETAILS

Mice

Mice were housed at the Pennsylvania State University College of Medicine and permitted unrestricted access to food and water. All experimental protocols were approved by the Pennsylvania State University College of Medicine's Institutional Animal Care and Use Committee. *Apc*^{Min}, UBC-Cre^{ERT}, and Confetti mice were obtained from Jackson Laboratories (C57BL/6J-Apc^{Min}/J stock no. 002020), (B6.Cg-Tg(UBC-cre/ERT2)1Ejb/1J stock no. 007001), (Gt(ROSA)26Sortm1(CAG-Brainbow2.1)Cle/J stock no. 137331). *Apc*$^{CKO/CKO}$ was obtained from the National Cancer Institute Mouse Repository (B6.Cg-*Apc*^{tm2Rak}/Nci strain no. 01XAA). MMTV-rtTA and TetO-Wnt1 transgenic lines were

maintained in a FVB/N background. All experimental mice were female. Experimental MMTV-rtTA/TetO-Wnt1/*Apc*^{Min} mice were obtained by crossing male *Apc*^{Min} to female MMTV-rtTA/TetO-Wnt1. Experimental MMTV-rtTA/TetO-Wnt1 mice were obtained by crossing male C57BL/6J to female MMTV-rtTA/TetO-Wnt1 for a consistent F_1 FVB/N-C57BL/6J genetic background. For doxycycline (dox) treatment, standard mouse chow was replaced with chow containing 2 g/kg drug (Bio Serv). Genotyping was performed via PCR using isolated genomic DNA from tail clips. UBC-Cre^{ERT}, Confetti, and *Apc*$^{CKO/CKO}$ as described from source. MMTV-rtTA and TetO-Wnt1 PCR using transgene specific primers (available upon request). All hosts were female F_1 FVB/N-C57BL/6J mice.

METHOD DETAILS

Primary tumor initiation, explants, and relapse

MMTV-rtTA/TetO-Wnt1 primary tumors and MMTV-rtTA/TetO-Wnt1/*Apc*^{min} primary tumors were initiated via *N-ethyl-N-nitrosourea* (ENU) (described below) exposure 1 week after beginning dox treatment with the exception of lineage A and B (Figure 3), which were spontaneous after ~6 months dox treatment. Explants were performed under isoflurane-induced anesthesia when a mammary tumor reached 2 × 2 cm (measured using calipers). Approximately 1/3 of the primary tumor was harvested and divided into ~2mm × 2mm fragments. Two fragments were used for biopsy histopathology and sequencing analysis. The rest were inserted via a small incision onto both flanks of a number of on-dox, female F_1 FVB/N-C57BL/6J (FVB/B6) host mice. Incisions were closed using surgical clips. All explant tumors were grown on dox until reaching 2 × 2 cm (~30–40 days). One mouse was taken for another generation of explants, and the remaining were removed from dox and monitored twice weekly for regression and relapse. The process was repeated over indicated generations. Time-to-relapse was noted as time between dox withdrawal and first post-withdrawal growth. When relapses reached 2 × 2 cm, explant hosts were necropsied, and relapses were cut using a razorblade into 18 segments. Each segment was stored separately at −80 C until sequencing.

DNA Preparation and Sanger Sequencing

Promega Maxwell 16 Tissue DNA Purification Kit (Promega AS1030) was used to isolate genomic DNA from tail snips and tumor fragments. Primers specific for *Apc*, *β-catenin*, and *rtTA* were used for PCR amplification. *Apc* primers listed in STAR Methods, b-*catenin*: 5′-

GCGTGGACAATGGCTACTCAA, 5′- GCGTCAAACTGCGTGGATGG, rtTA: 5′-GCCCAGAAGCTAGGTGTAG, 5′-CGAATAAGAA GGCTGGCTCTGC. PCR products were purified using a Qiaquick PCR purification kit (28104) or Affimetrix ExoSAP-IT (P/N: 75001). Purified products were Sanger sequenced at *Genewiz LLC*, South Plainfield, NJ, USA.

Chemical Carcinogenesis

N-methyl-N-nitrosourea (MNU) or *N-ethyl-N-nitrosourea* (ENU) were given via intraperitoneal (i.p.) injection (150mg/kg) at 7 weeks of age for select primary mice. For explants, injections were administered when tumors reached 1.5 ×1.5 cm. MNU (Sigma

Aldrich N4766) was dissolved in 10mg/mL 0.9% saline immediately prior to injection, and 1g ENU (Sigma Aldrich N3385) was dissolved in 10 mL 95% ethanol and 90mL phosphocitrate buffer (Sigma Aldrich P4809) immediately prior to injection.

High throughput sequencing

An *Apc*^{mmcr} PCR product was amplified using primers designed to add the following adapters. 5′-TCGTCGGCAGCGTCAGATGTGTATAAGA GACAGACAGAAAGTACTCCAGACGGG-3′, and 5′-GTCTCGTGGGCTCGGAGATGTGTATAAGAGACAGTGGCTTGGCG TGAT

GACTTTG-3′. Followed Illumina 16S Metagenomic Sequencing Library Preparation Protocol for clean-up, quantification and normalization. Indices were added using Nextera XT index kit # FC-131–1001. Samples were sequenced using the Illumina Miseq platform, 250 3 250 paired end. Targeted deep sequencing of the amplicon resulted in an average of 287,000 reads per base pair between *Apc* codons 1492 and 1580. Reads were converted to percentages by dividing the number of reads per base pair at each site by the total number of reads at each site. For example, if a specific site with reference G produced the following: A: 1450 reads, T: 6000 reads G: 242,430 reads, C: 120 reads, it was converted to: A: 0.58%, T: 2.4%, G: 97.0%, C: 0.05%. Next, we estimated error at each site by analyzing the read percentages from the average of two samples known to harbor no mutations, and subtracted that percentage from the experimental samples. Thus, supposing the “no mutations” sample at the above hypothetical G site read the following: A: 0.56%, T: 0.64%, G: 98.73%, C: 0.07%, we subtracted those percentages from the experimental sample to estimate the true variant allele frequency as: A: 0.02%, T: 1.76%, G: 1.73%, C: 0.02%. The hypothetical data here indicate a G > T variant in 1.76% of the sample. In this way, we were able to detect mutants with a mutant allele fraction > 0.3%. Ability to detect these low frequency mutants was corroborated by the fact that the mutants identified were nearly always nonsense mutations and consistent with the known ENU mutation pattern.

Quantitative Real Time PCR

RNA was purified from mammary glands or tumor fragments using Promega Maxwell 16 Tissue RNA Purification Kit (Promega AS1050) and reverse transcribed using Invitrogen Superscript First Strand Synthesis kit (15080051). We used Taqman Gene Expression Assay Mix (Agilent, Cat#600880) to measure expression of Wnt1 (Applied Biosystems, Mm_01300555_g1). The mix contained unlabeled PCR primers and FAM-labeled probes. Relative quantification PCR (ΔΔCt method) was performed with duplicate reactions using Algilent Technologies Mx3005P detection system and analyzed using Stratagene MxPro Software. Expression levels of Wnt1 were normalized to Gapdh transcript levels (Biosystems 435239E).

Bacterial subcloning

PCR product was purified using a Qiaquick PCR purification kit (28104) and subcloned using One Shot TOP 10 chemically competent cells (Invitrogen C404004) and TOPO XL PCR Cloning Kit (Invitrogen 45–0008LT). Multiple individual colonies positive for the insert were harvested and lysed using 10ul water. Second PCR amplification from plasmid

DNA was done using the same primers above and purified again. Products were sequenced at *Genewiz LLC*, South Plainfield, NJ, USA.

Cell suspensions and tumor reconstitution

A tumor relapse (composed of R1 and R2 cell populations), as well as the parental iWnt/ Apc^{Min} tumor were made to single cell suspensions. First, ~10×10mm fragments of mammary tumor tissue were finely chopped and scraped into a sterile tube. To each, we added 1mL 10X collaganse (diluted in 1X PBS, 63.29mg/5mL) (Sigma C9891), 1mL Hyaluronidase (diluted in 1X PBS, 44.36mg/10mL) (Sigma H3506), and 8 mL DMEM/F12 media. Tissue was incubated for 1 hour at 37 C while slowly shaking, then centrifuged at 550xg for 5 minutes. The pellet was re-suspend in 7mL 0.25% Trypsin-EDTA (GIBCO 15000–054) and shaken vigorously by hand for 1–3 minutes until tissue chunks were broken. Next, the tissue was centrifuged again and the supernatant removed. The pellet was re-suspended in 2mL pre-warmed, sterile-filtered 1X Dispase / Neutral Protease (10mg/mL) (Roche 0492078001) + 0.4 mL 10X DNase (Worthington DNase-DPRF LS006331) + 1.6 mL 1X PBS and shaken by hand for 1–3 minutes. Cells were filtered into 5mL tubes with 40μm filter caps (Falcon cat#352235) and then centrifuged for 5 minutes at 550xg. Finally, pellet was re-suspend in 0.64% $NHCl_4$, incubated at room temperature for 3 minutes, then centrifuged at 550xg for 5 minutes and re-suspend in 1X PBS. Cells were counted a hemocytometer, and re-suspend in 50% PBS, 50% Matrigel (BD Biosciences Growth Factor Reduced Matrigel Mix, Cat#356231) at 1,000 cells/μL for mammary gland injections. Mammary glands were exposed via surgical incision, and 10^5 cells in 100μL Matrigel/PBS were injected into intact 3 or 4 mammary fat pads of on-dox, host FVB/B6 female mice. In mixed population injections, cells were injected in a 2:1 admixture (R1:R2 or P:R2, respectively). Growth occurred synchronously and tumors were harvested at 31 days post injection, when multiregion sequencing was feasible for all tumors.

Tamoxifen

Tamoxifen (Sigma T5648–1G) was dissolved in corn oil (Sigma C8267) at 20mg/mL. 3 mg was injected intraperitoneally for Cre-mediated recombination.

Confocal Imaging

Snap frozen sections of tumors (mammary or intestine) (~20μm) were cut and mounted on slides. DRAQ5 (Cell Signaling 4084S) was used as a counterstain for far-red fluorescence. Slides were visualized using a Leica SP8 Inverted Confocal Microscope and analyzed using IMARIS Florescence imaging processing software.

Immunohistochemistry

Mammary glands, mammary tumors, and intestinal tumors were fixed with 4% paraformaldehyde for at least 2 hours, imbedded in paraffin, and sectioned. Samples were heated to 65C for 20 minutes in PBS and cooled for 20 minutes at room temperature. They were cleared with 3× 5 minutes incubation in xylene and rehydrated with 2× 1 minute 100% ethanol, 2× 2 minutes 95% ethanol, and 1× 1 minute 70% ethanol, then placed in PBS for 10 minutes. Antigen retrieval was accomplished via incubation in Sodium Citrate Buffer pH 6.0

for 1 hour at 80C. Samples were then cooled for 10 minutes prior to being washed in PBS at room temperature while slowly shaking. The DAKO envision ARK kit (#3954) was utilized for β-catenin immunohistochemistry. Briefly, endogenous peroxidase activity was quenched for 5 minutes at room temperature with peroxidase block. The primary antibody (mouse anti-β-catenin, BD Transduction Laboratories, 610153) was conjugated to a biotinylated secondary antibody for 15 minutes at room temperature. Then, the blocking reagent containing mouse serum was added to bind residual Biotinylation Reagent. The mixture containing the primary antibody, biotinylated secondary antibody, and mouse serum was diluted to a final primary antibody concentration of 1:50 with PBS 0.1% Triton X and incubated overnight at 4C in the dark. The following day, samples were washed for 10 minutes in PBS and incubated with streptavidin peroxidase for 15 minutes at room temperature then washed for 10 minutes in PBS and developed with 3′3-diaminobenidine (DAB) + substrate-chromagen for 10 minutes at room temperature. Finally, samples were washed in water for 5 minutes, 95% ethanol 2× 2 minutes, 100% ethanol 2× 2 minutes, and xylene 3× 1 minutes. Samples were then coverslipped and visualized.

QUANTIFICATION AND STATISTICAL ANALYSIS

Student's t test and Log Rank Test were performed using GraphPad Prism 6.04. Fisher's Exact Probability Tests (2×2 and 2×3 tables) were performed using VassarStats: Website for Statistical Computation. http://vassarstats.net/. n values are reported in figure legends.

Supplementary Material

Refer to Web version on PubMed Central for supplementary material.

ACKNOWLEDGMENTS

We thank Aswathy Sebastian and Istvan Albert of the Penn State Bioinformatics Consulting Center for expert help with processing and analyzing of Illumina sequencing outputs. High-throughput sequencing was performed through the Penn State Genomics Core Facility (University Park, PA, USA). We thank members of the Gunther laboratory for critical review of the manuscript. This work was supported by grants from the National Cancer Institute (R01 CA152222 and R01 CA212584) and funding received from the benefactors of the Jake Gittlen Laboratories for Cancer Research. Animal housing was provided through a facility constructed with support from a Research Facilities Improvement Grant (C06 RR-15428–01) from the National Center for Research Resources.

REFERENCES

Albuquerque C, Breukel C, van der Luijt R, Fidalgo P, Lage P, Slors FJ, Leitão CN, Fodde R, and Smits R (2002). The 'just-right' signaling model: APC somatic mutations are selected based on a specific level of activation of the beta-catenin signaling cascade. Hum. Mol. Genet 11, 1549–1560. [PubMed: 12045208]

Ambrogio C, Barbacid M, and Santamaría D (2017). In vivo oncogenic conflict triggered by co-existing KRAS and EGFR activating mutations in lung adenocarcinoma. Oncogene 36, 2309–2318. [PubMed: 27775074]

Amin AD, Rajan SS, Groysman MJ, Pongtornpipat P, and Schatz JH (2015a). Oncogene overdose: too much of a bad thing for oncogene-addicted cancer cells. Biomark. Cancer 7 (Suppl 2), 25–32.

Amin AD, Rajan SS, Liang WS, Pongtornpipat P, Groysman MJ, Tapia EO, Peters TL, Cuyugan L, Adkins J, Rimsza LM, et al. (2015b). Evidence suggesting that discontinuous dosing of ALK kinase inhibitors may prolong control of ALK+ tumors. Cancer Res. 75, 2916–2927. [PubMed: 26018086]

Bakker ER, Hoekstra E, Franken PF, Helvensteijn W, van Deurzen CH, van Veelen W, Kuipers EJ, and Smits R (2013). β-catenin signaling dosage dictates tissue-specific tumor predisposition in Apc-driven cancer. Oncogene 32, 4579–4585. [PubMed: 23045279]

Bhang HE, Ruddy DA, Krishnamurthy Radhakrishna V, Caushi JX, Zhao R, Hims MM, Singh AP, Kao I, Rakiec D, Shaw P, et al. (2015). Studying clonal dynamics in response to cancer therapy using high-complexity barcoding. Nat. Med 21, 440–448. [PubMed: 25849130]

Bozic I, Reiter JG, Allen B, Antal T, Chatterjee K, Shah P, Moon YS, Yaqubie A, Kelly N, Le DT, et al. (2013). Evolutionary dynamics of cancer in response to targeted combination therapy. eLife 2, e00747. [PubMed: 23805382]

Brammeld JS, Petljak M, Martincorena I, Williams SP, Alonso LG, Dalmases A, Bellosillo B, Robles-Espinoza CD, Price S, Barthorpe S, et al. (2017). Genome-wide chemical mutagenesis screens allow unbiased saturation of the cancer genome and identification of drug resistance mutations. Genome Res. 27, 613–625. [PubMed: 28179366]

Buchert M, Athineos D, Abud HE, Burke ZD, Faux MC, Samuel MS, Jarnicki AG, Winbanks CE, Newton IP, Meniel VS, et al. (2010). Genetic dissection of differential signaling threshold requirements for the Wnt/beta-catenin pathway in vivo. PLoS Genet. 6, e1000816. [PubMed: 20084116]

Burrell RA, and Swanton C (2014). Tumour heterogeneity and the evolution of polyclonal drug resistance. Mol. Oncol 8, 1095–1111. [PubMed: 25087573]

Bystrykh LV, and Belderbos ME (2016). Clonal analysis of cells with cellular barcoding: when numbers and sizes matter. Methods Mol. Biol 1516, 57–89. [PubMed: 27044044]

Cleary AS, Leonard TL, Gestl SA, and Gunther EJ (2014). Tumour cell heterogeneity maintained by cooperating subclones in Wnt-driven mammary cancers. Nature 508, 113–117. [PubMed: 24695311]

Das Thakur M, Salangsang F, Landman AS, Sellers WR, Pryer NK, Levesque MP, Dummer R, McMahon M, and Stuart DD (2013). Modelling vemurafenib resistance in melanoma reveals a strategy to forestall drug resistance. Nature 494, 251–255. [PubMed: 23302800]

Debies MT, Gestl SA, Mathers JL, Mikse OR, Leonard TL, Moody SE, Chodosh LA, Cardiff RD, and Gunther EJ (2008). Tumor escape in a Wnt1-dependent mouse breast cancer model is enabled by p19Arf/p53 pathway lesions but not p16 Ink4a loss. J. Clin. Invest 118, 51–63. [PubMed: 18060046]

Diaz LA, Jr., Williams RT, Wu J, Kinde I, Hecht JR, Berlin J, Allen B, Bozic I, Reiter JG, Nowak MA, et al. (2012). The molecular evolution of acquired resistance to targeted EGFR blockade in colorectal cancers. Nature 486, 537–540. [PubMed: 22722843]

Dow LE, O'Rourke KP, Simon J, Tschaharganeh DF, van Es JH, Clevers H, and Lowe SW (2015). Apc restoration promotes cellular differentiation and reestablishes crypt homeostasis in colorectal cancer. Cell 161, 1539–1552. [PubMed: 26091037]

Enriquez-Navas PM, Kam Y, Das T, Hassan S, Silva A, Foroutan P, Ruiz E, Martinez G, Minton S, Gillies RJ, and Gatenby RA (2016). Exploiting evolutionary principles to prolong tumor control in preclinical models of breast cancer. Sci. Transl. Med 8, 327ra24.

Gaspar C, Franken P, Molenaar L, Breukel C, van der Valk M, Smits R, and Fodde R (2009). A targeted constitutive mutation in the APC tumor suppressor gene underlies mammary but not intestinal tumorigenesis. PLoS Genet. 5, e1000547. [PubMed: 19578404]

Gatenby RA, Silva AS, Gillies RJ, and Frieden BR (2009). Adaptive therapy. Cancer Res. 69, 4894–4903. [PubMed: 19487300]

Gerlinger M, Rowan AJ, Horswell S, Math M, Larkin J, Endesfelder D, Gronroos E, Martinez P, Matthews N, Stewart A, et al. (2012). Intratumor heterogeneity and branched evolution revealed by multiregion sequencing. N. Engl. J. Med 366, 883–892. [PubMed: 22397650]

Gunther EJ, Moody SE, Belka GK, Hahn KT, Innocent N, Dugan KD, Cardiff RD, and Chodosh LA (2003). Impact of p53 loss on reversal and recurrence of conditional Wnt-induced tumorigenesis. Genes Dev. 17, 488–501. [PubMed: 12600942]

Haddow A, Watkinson JM, Paterson E, and Koller PC (1944). Influence of synthetic oestrogens on advanced malignant disease. BMJ 2, 393–398. [PubMed: 20785660]

Haigis KM, and Dove WF (2003). A Robertsonian translocation suppresses a somatic recombination pathway to loss of heterozygosity. Nat. Genet 33, 33–39. [PubMed: 12447373]

Hata AN, Niederst MJ, Archibald HL, Gomez-Caraballo M, Siddiqui FM, Mulvey HE, Maruvka YE, Ji F, Bhang HE, Krishnamurthy Radhakrishna V, et al. (2016). Tumor cells can follow distinct evolutionary paths to become resistant to epidermal growth factor receptor inhibition. Nat. Med 22, 262–269. [PubMed: 26828195]

Hughes D, and Andersson DI (2015). Evolutionary consequences of drug resistance: shared principles across diverse targets and organisms. Nat. Rev. Genet 16, 459–471. [PubMed: 26149714]

Jansen JG, Mohn GR, Vrieling H, van Teijlingen CM, Lohman PH, and van Zeeland AA (1994a). Molecular analysis of hprt gene mutations in skin fibroblasts of rats exposed in vivo to N-methyl-N-nitrosourea or N-ethyl-N-nitrosourea. Cancer Res. 54, 2478–2485. [PubMed: 8162597]

Jansen JG, van Teijlingen CM, Mohn GR, van Zeeland AA, and Vrieling H (1994b). AT base pairs are the main target for mutations at the hprt locus of rat skin fibroblasts exposed in vitro to the monofunctional alkylating agent N-ethyl-N-nitrosourea. Mutagenesis 9, 417–421. [PubMed: 7837975]

Jordan VC, and Ford LG (2011). Paradoxical clinical effect of estrogen on breast cancer risk: a “new” biology of estrogen-induced apoptosis. Cancer Prev. Res. (Phila.) 4, 633–637. [PubMed: 21478501]

Juric D, Castel P, Griffith M, Griffith OL, Won HH, Ellis H, Ebbesen SH, Ainscough BJ, Ramu A, Iyer G, et al. (2015). Convergent loss of PTEN leads to clinical resistance to a PI(3)Ka inhibitor. Nature 518, 240–244. [PubMed: 25409150]

Keller RR, Gestl SA, Lu AQ, Hoke A, Feith DJ, and Gunther EJ (2016). Carcinogen-specific mutations in preferred Ras-Raf pathway onco-genes directed by strand bias. Carcinogenesis 37, 810–816. [PubMed: 27207659]

Kielman MF, Rindapa¨a¨ M, Gaspar C, van Poppel N, Breukel C, van Leeuwen S, Taketo MM, Roberts S, Smits R, and Fodde R (2002). Apc modulates embryonic stem-cell differentiation by controlling the dosage of beta-catenin signaling. Nat. Genet 32, 594–605. [PubMed: 12426568]

Kong X, Kuilman T, Shahrabi A, Boshuizen J, Kemper K, Song JY, Niessen HWM, Rozeman EA, Geukes Foppen MH, Blank CU, and Peeper DS (2017). Cancer drug addiction is relayed by an ERK2-dependent phenotype switch. Nature 550, 270–274. [PubMed: 28976960]

Kuraguchi M, Wang XP, Bronson RT, Rothenberg R, Ohene-Baah NY, Lund JJ, Kucherlapati M, Maas RL, and Kucherlapati R (2006). Adeno matous polyposis coli (APC) is required for normal development of skin and thymus. PLoS Genet. 2, e146. [PubMed: 17002498]

Kuraguchi M, Ohene-Baah NY, Sonkin D, Bronson RT, and Kucherlapati R (2009). Genetic mechanisms in Apc-mediated mammary tumorigenesis. PLoS Genet. 5, e1000367. [PubMed: 19197353]

McGranahan N, and Swanton C (2017). Clonal heterogeneity and tumor evolution: past, present, and the future. Cell 168, 613–628. [PubMed: 28187284]

Misale S, Yaeger R, Hobor S, Scala E, Janakiraman M, Liska D, Valtorta E, Schiavo R, Buscarino M, Siravegna G, et al. (2012). Emergence of KRAS mutations and acquired resistance to anti-EGFR therapy in colorectal cancer. Nature 486, 532–536. [PubMed: 22722830]

Moser AR, Mattes EM, Dove WF, Lindstrom MJ, Haag JD, and Gould MN (1993). ApcMin, a mutation in the murine Apc gene, predisposes to mammary carcinomas and focal alveolar hyperplasias. Proc. Natl. Acad. Sci. USA 90, 8977–8981. [PubMed: 8415640]

Nieto P, Ambrogio C, Esteban-Burgos L, Gómez-López G, Blasco MT, Yao Z, Marais R, Rosen N, Chiarle R, Pisano DG, et al. (2017). A Braf kinase-inactive mutant induces lung adenocarcinoma. Nature 548, 239–243. [PubMed: 28783725]

Nik-Zainal S, Davies H, Staaf J, Ramakrishna M, Glodzik D, Zou X, Martincorena I, Alexandrov LB, Martin S, Wedge DC, et al. (2016). Landscape of somatic mutations in 560 breast cancer whole-genome sequences. Nature 534, 47–54. [PubMed: 27135926]

Premsrirut PK, Dow LE, Kim SY, Camiolo M, Malone CD, Miething C, Scuoppo C, Zuber J, Dickins RA, Kogan SC, et al. (2011). A rapid and scalable system for studying gene function in mice using conditional RNA interference. Cell 145, 145–158. [PubMed: 21458673]

Probst FJ, and Justice MJ (2010). Mouse mutagenesis with the chemical supermutagen ENU. Methods Enzymol. 477, 297–312. [PubMed: 20699147]

Rowan AJ, Lamlum H, Ilyas M, Wheeler J, Straub J, Papadopoulou A, Bicknell D, Bodmer WF, and Tomlinson IP (2000). APC mutations in sporadic colorectal tumors: a mutational "hotspot" and interdependence of the "two hits". Proc. Natl. Acad. Sci. USA 97, 3352–3357. [PubMed: 10737795]

Ruzankina Y, Pinzon-Guzman C, Asare A, Ong T, Pontano L, Cotsarelis G, Zediak VP, Velez M, Bhandoola A, and Brown EJ (2007). Deletion of the developmentally essential gene ATR in adult mice leads to age-related phenotypes and stem cell loss. Cell Stem Cell 1, 113–126. [PubMed: 18371340]

Sarkisian CJ, Keister BA, Stairs DB, Boxer RB, Moody SE, and Chodosh LA (2007). Dose-dependent oncogene-induced senescence in vivo and its evasion during mammary tumorigenesis. Nat. Cell Biol. 9, 493–505. [PubMed: 17450133]

Schweizer MT, Antonarakis ES, Wang H, Ajiboye AS, Spitz A, Cao H, Luo J, Haffner MC, Yegnasubramanian S, Carducci MA, et al. (2015). Effect of bipolar androgen therapy for asymptomatic men with castration-resistant prostate cancer: results from a pilot clinical study. Sci. Transl. Med 7, 269ra2.

Serrano M, Lin AW, McCurrach ME, Beach D, and Lowe SW (1997). Oncogenic ras provokes premature cell senescence associated with accumulation of p53 and p16INK4a. Cell 88, 593–602. [PubMed: 9054499]

Siravegna G, Mussolin B, Buscarino M, Corti G, Cassingena A, Crisafulli G, Ponzetti A, Cremolini C, Amatu A, Lauricella C, et al. (2015). Clonal evolution and resistance to EGFR blockade in the blood of colorectal cancer patients. Nat. Med 21, 827.

Snippert HJ, van der Flier LG, Sato T, van Es JH, van den Born M, Kroon-Veenboer C, Barker N, Klein AM, van Rheenen J, Simons BD, and Clevers H (2010). Intestinal crypt homeostasis results from neutral competition between symmetrically dividing Lgr5 stem cells. Cell 143, 134–144. [PubMed: 20887898]

Stewart TA, Pattengale PK, and Leder P (1984). Spontaneous mammary adenocarcinomas in transgenic mice that carry and express MTV/myc fusion genes. Cell 38, 627–637. [PubMed: 6488314]

Sun C, Wang L, Huang S, Heynen GJ, Prahallad A, Robert C, Haanen J, Blank C, Wesseling J, Willems SM, et al. (2014). Reversible and adaptive resistance to BRAF(V600E) inhibition in melanoma. Nature 508, 118–122. [PubMed: 24670642]

Toki H, Inoue M, Motegi H, Minowa O, Kanda H, Yamamoto N, Ikeda A, Karashima Y, Matsui J, Kaneda H, et al. (2013). Novel mouse model for Gardner syndrome generated by a large-scale N-ethyl-N-nitrosourea muta-genesis program. Cancer Sci. 104, 937–944. [PubMed: 23551873]

Turke AB, Zejnullahu K, Wu YL, Song Y, Dias-Santagata D, Lifshits E, Toschi L, Rogers A, Mok T, Sequist L, et al. (2010). Preexistence and clonal selection of MET amplification in EGFR mutant NSCLC. Cancer Cell 17, 77–88. [PubMed: 20129249]

Unni AM, Lockwood WW, Zejnullahu K, Lee-Lin SQ, and Varmus H (2015). Evidence that synthetic lethality underlies the mutual exclusivity of oncogenic KRAS and EGFR mutations in lung adenocarcinoma. eLife 4, e06907. [PubMed: 26047463]

Varmus H, Unni AM, and Lockwood WW (2016). How cancer genomics drives cancer biology: does synthetic lethality explain mutually exclusive oncogenic mutations? Cold Spring Harb. Symp. Quant. Biol 81, 247–255. [PubMed: 28123049]

Weinstein IB (2002). Cancer. Addiction to oncogenes–the Achilles heal of cancer. Science 297, 63–64. [PubMed: 12098689]

Westcott PM, Halliwill KD, To MD, Rashid M, Rust AG, Keane TM, Delrosario R, Jen KY, Gurley KE, Kemp CJ, et al. (2015). The mutational landscapes of genetic and chemical models of Kras-driven lung cancer. Nature 517, 489–492. [PubMed: 25363767]

Zhang J, Cunningham JJ, Brown JS, and Gatenby RA (2017). Integrating evolutionary dynamics into treatment of metastatic castrate-resistant prostate cancer. Nat. Commun 8, 1816. [PubMed: 29180633]

Highlights

- Wnt-driven mammary cancers maintain dependence on sub-maximal Wnt signaling
- Rescue mutations destined to subvert targeted therapy carry a fitness cost
- Oncogene overdose imposes negative selection, leading to turnover of rescue subclones

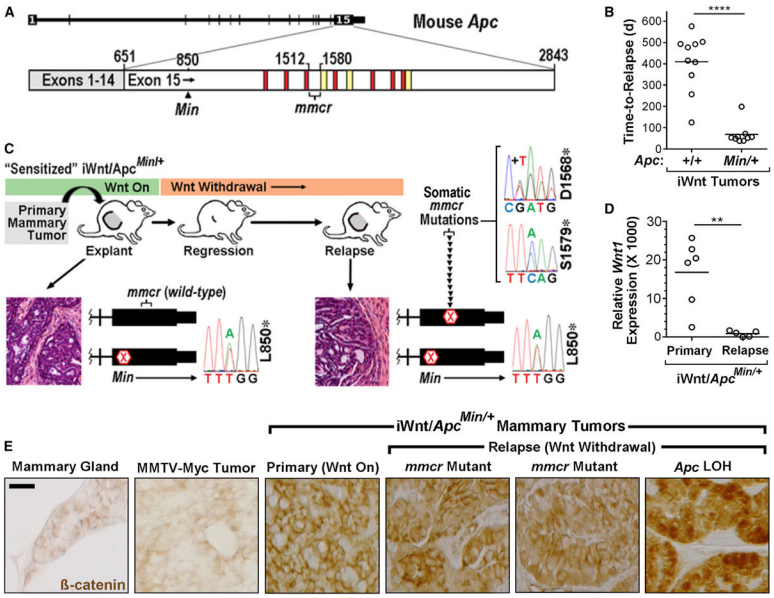

Figure 1. Stringent Selection for Hypomorphic, Second-Hit *Apc*^{mmcr} Rescue Mutations at Relapse

(A) *Apc* gene map. Nonsense mutations within the *Apc*^{mmcr} region create truncations that eliminate all three Ser-Ala-Met-Pro (SAMP) repeats (yellow) while retaining three of seven 20-amino-acid (aa) β-cat binding-degradation repeats (red).

(B) Accelerated relapse onset in *Apc*$^{Min/+}$ versus *Apc*$^{+/+}$ iWnt tumor explants.

(C) Somatic, second-hit *Apc*^{mmcr} rescue mutations in iWnt/*Apc*$^{Min/+}$ mammary tumor relapses. Chromatogram snapshots depict representative relapse-specific *Apc*^{mmcr} mutations. Both tumor histopathology and *Apc*^{Min} heterozygosity are preserved from primary tumor to relapse.

(D) Expression of *Wnt1* transcripts relative to *Gapdh* in primary versus relapsed iWnt/*Apc*$^{Min/+}$ tumor explants as determined by qRT-PCR.

(E) β-cat immunostaining of tissue and tumor sections.

**p < 0.01; ****p < 0.0001 by unpaired, two-tailed t test. Scale bar, 50 μm.

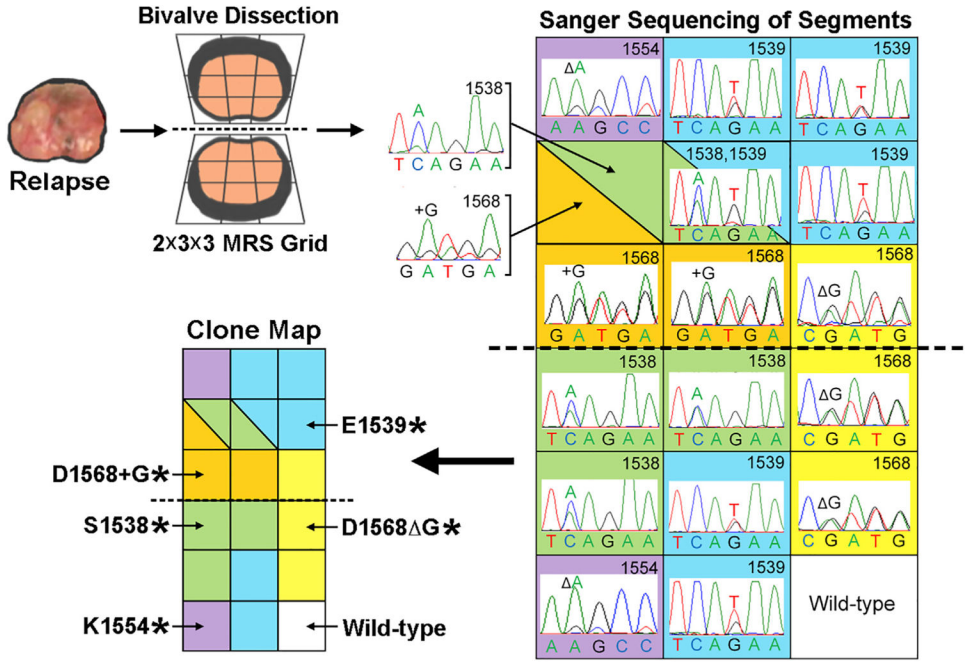

Figure 2. Polyclonal Relapse Uncovered by MRS Analysis of the *Apc*^{mmcr}

Schematic depicts the protocol for analyzing relapsed mammary tumors by MRS. Chromatogram snapshots depict *Apc*^{mmcr} rescue mutations detected by Sanger sequencing in each segment of a representative relapse. The aggregate MRS analysis was used to construct a color-coded subclone map, in which segments sharing the same rescue mutation are color matched. Split segments denote detection of two distinct rescue mutations co-residing in a single segment. The subclone map is depicted in “bivalve view” such that folding the map at the dotted midline overlays the original 3 × 3 segmented halves in register.

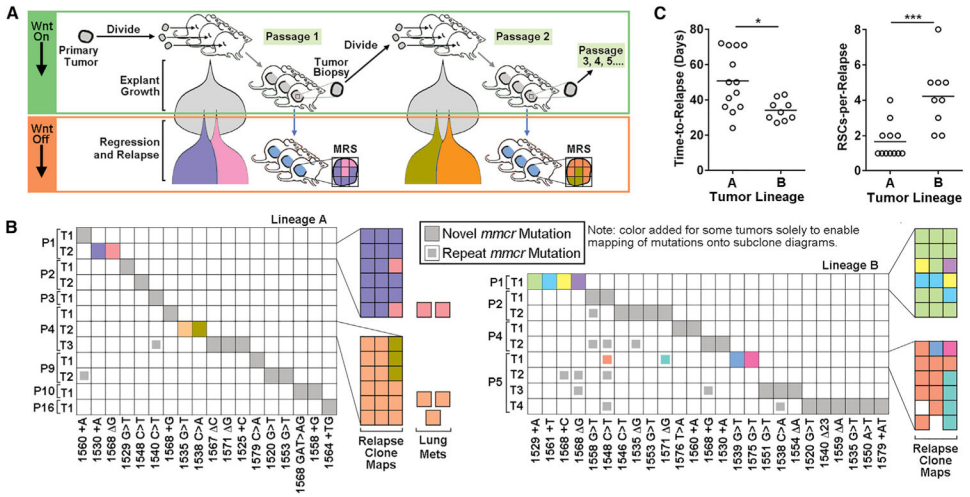

Figure 3. No Accumulation of *Apc*^{mmcr} Rescue Mutations on Serial Passage of iWnt/*Apc*$^{Min/+}$ Tumors

(A) Schematic. Illustration depicts serial passage of iWnt/*Apc*$^{Min/+}$ tumor lineages and detection of RSCs at relapse across multiple generations. Expansion of tumor subclones at each passage is depicted by Muller diagrams.

(B) Tiling plots. Relapsed tumors (T) analyzed at the indicated passage (P) were analyzed by MRS to elucidate subclone composition. *Apc*^{mmcr} rescue mutations are arrayed along the x axis. Subclone maps for representative relapses are depicted to the right of each tiling plot, with 3-by-6 grids depicting bivalve views of individual relapses. An unfilled (white) box indicates no *Apc*^{mmcr} mutation was detected by Sanger DNA sequencing, whereas an unbounded area indicates a missing segment owing to irregular tumor shape or a pocket of necrosis.

(C) Dot plots depicting time to relapse onset (left) and RSCs per relapse (right) for each tumor lineage.

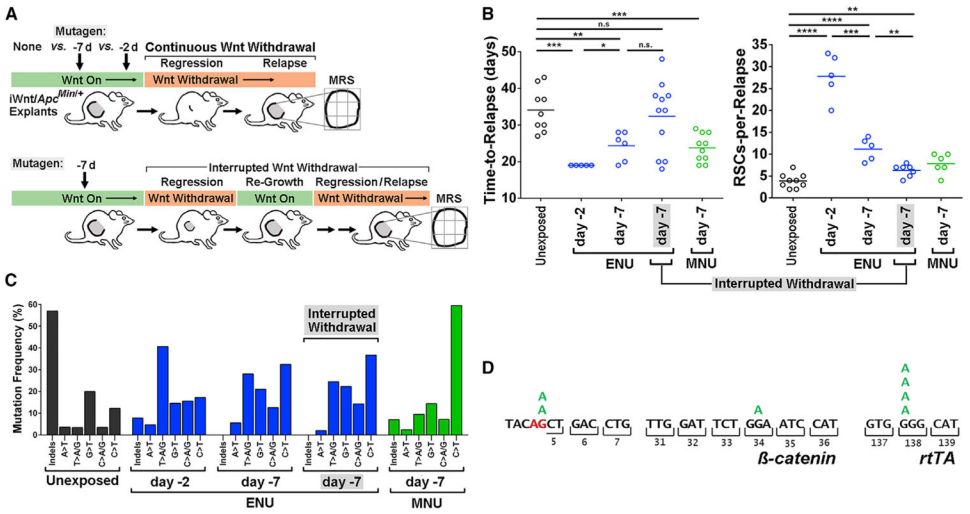

Figure 4. Rapid Turnover of *Apc*^{mmcr} Mutant RSCs Generated by Mutagen Exposure

(A) Experimental design.

(B) Time to relapse and RSCs per relapse (as determined by MRS analysis) following timed mutagen exposure. See also Figures S4 and S5.

(C) *Apc*^{mmcr} rescue mutation spectra obtained under various exposure conditions. Unexposed, n = 109 *Apc*^{mmcr} mutations; day −2 ENU, n = 66; day −7 ENU, n = 72; day −7 ENU/interrupted withdrawal, n = 44; day −7 MNU, n = 44.

(D) Alternative G > A rescue mutations detected in MNU-exposed relapse segments that lack an *Apc*^{mmcr} rescue mutation.

*p < 0.05; **p < 0.01; ***p < 0.001; t test.

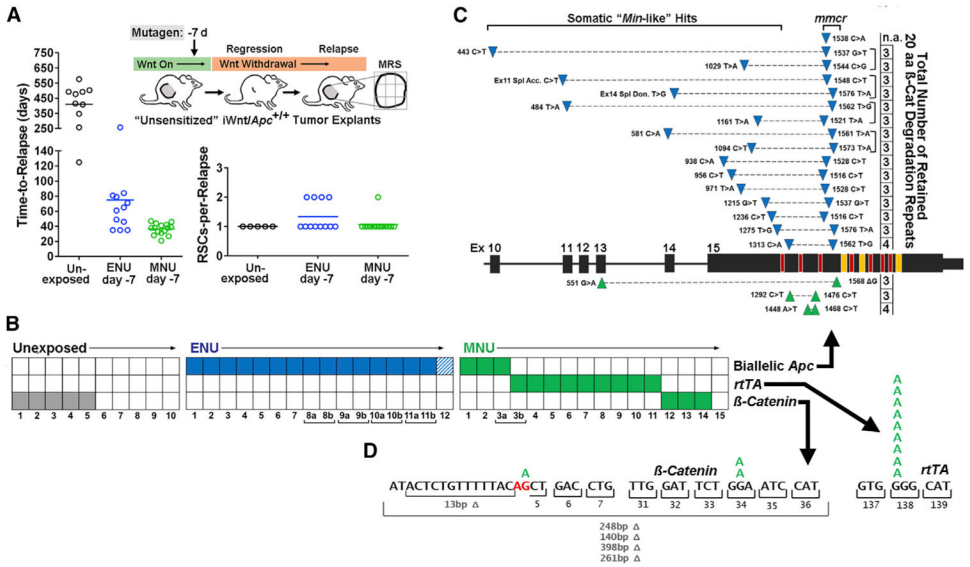

Figure 5. Unsensitized, Mutagen-Exposed iWnt/*Apc*$^{+/+}$ Relapses Converge on Sub-maximum Wnt Signaling via Biallelic *Apc* Rescue Mutations

(A) Time to relapse and RSCs per relapse by exposure condition.

(B) Mutual exclusivity of *Apc*, *βcat*, and *rtTA* rescue mutations. Co-occurrence plots depicting modes of relapse for each exposure condition. Relapses with "a" and "b" designations harbored two distinct subclones when analyzed by MRS (see also Figure S5). Hatched box indicates the sole instance where an *Apc*^{mmcr} mutation was detected without an accompanying upstream mutation.

(C) Map of biallelic *Apc* rescue mutations. Mutation pairs converge on retention of 3 or 4 *β*-cat degradation domains, summed across the two alleles.

(D) MNU-induced G > A changes, which cannot generate *Apc*^{mmcr} nonsense mutations due to coding constraints, instead generate rescue mutations targeting *β*-cat and *rtTA*.

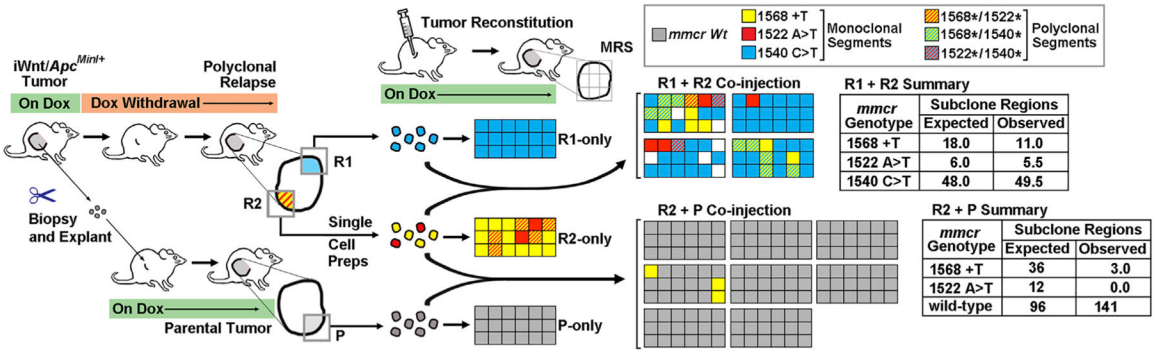

R1 + R2 Summary

mmcr Genotype	Subclone Regions	
	Expected	Observed
1568 +T	18.0	11.0
1522 A>T	6.0	5.5
1540 C>T	48.0	49.5

R2 + P Summary

mmcr Genotype	Subclone Regions	
	Expected	Observed
1568 +T	36	3.0
1522 A>T	12	0.0
wild-type	96	141

Figure 6. *Apc*^{mmcr} Mutant RSCs Outcompeted by Parental Tumor Cells

The cartoon at left depicts the experimental strategy for comparing clone contribution during competitive tumor reconstitution. Experimental results are depicted as subclone maps (color-coded 3 × 6 grids as in Figure 2 but with the bivalve “fold” rotated 90 degrees). Each map depicts the MRS analysis performed on a single reconstituted tumor (n = 4 for R1 + R2 co-injection; n = 8 for R2 + P co-injection). The key at top right indicates the color assignment for each *Apc*^{mmcr} mutation. Upper panels: neutral competition between R1 and R2 relapse cell populations is shown. Subclone map analysis shows that the number of segments bearing R1-specific versus R2-specific mutant alleles was comparable to the number expected based on the ratio of R1:R2 cells within the injected admixture (no significant variation from expected clone contribution; $p = 0.48$; Fisher’s exact test with Freeman-Halton extension; 5.5 segments rounded to 6.0; 49.5 rounded to 50). Lower panels: P cells outcompete R2 cells. The number of segments bearing R2-specific mutant alleles is significantly less than the number expected based on the ratio of R2:P cells within the injected admixture ($p < 0.0001$; Fisher’s exact test with Freeman-Halton extension).

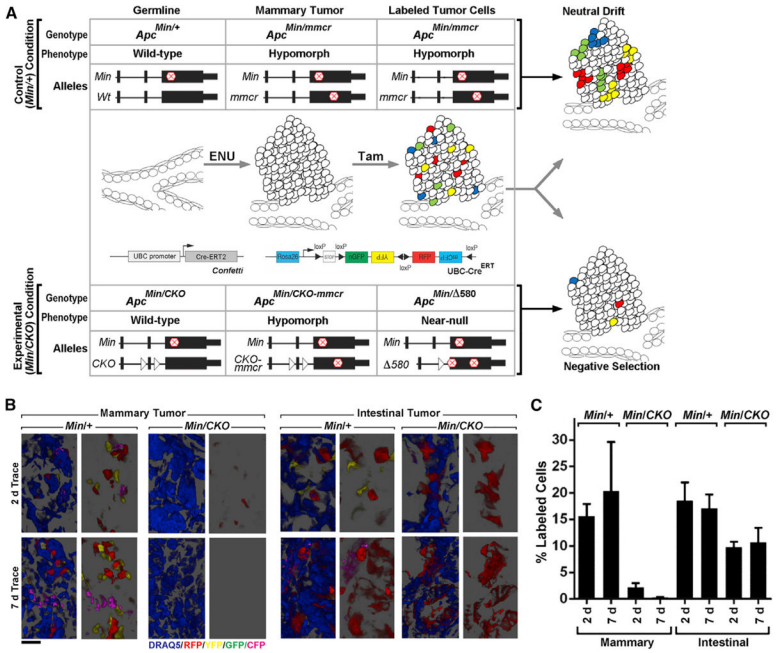

Figure 7. Dropout of Mammary Tumor Cells upon *Apc*^{mmcr} to *Apc*$^{\Delta 580}$ Conversion

(A) Schematic depicting the experimental strategy.

(B) Tumor cell lineage tracing at clonal density. Mice of the indicated *Apc* genotypes were treated with Tam to generate *Confetti*-labeled clones within mammary and intestinal tumors. Tumor samples collected at days 2 and 7 of the trace then were analyzed by confocal microscopy to assess clone perdurance. Panels depict representative confocal microscopy images of tumor sections at the indicated time points. Mammary tumors carrying the germline *Apc*^{CKO} allele show dropout of *Confetti*-labeled clones, coincident with Cre-mediated conversion of the tumor cell genotype from *Apc*$^{Min/CKO\text{-}mmcr}$ to *Apc*$^{Min/\Delta 580}$ (see also Figure S7).

(C) Quantification of the confocal imaging data depicted in (A). n = 3 tumors per condition. At minimum, 470 cells were scored for each tumor, and 2,200 cells were scored for each condition. Error bars, SEM.

Scale bar, 100 μm.

KEY RESOURCES TABLE

REAGENT or RESOURCE Antibodies	SOURCE	IDENTIFIER
Antibodies		
Mouse monoclonal anti-β-catenin	BD Transduction Laboratories	Cat# 1610153
Chemicals, Peptides, and Recombinant Proteins		
N-methyl-N-nitrosourea (MNU)	Sigma Aldrich	N4766
N-ethyl-N-nitrosourea (ENU)	Sigma Aldrich	N3385
Tamoxifen	Sigma Aldrich	T5648–1G
Critical Commercial Assays		
PCR purification kit	Qiaquick	28104
ExoSAP-IT	Affimetrix	P/N: 75001
Taqman Gene Expression Assay Mix	Agilent	Cat#600880
One Shot TOP 10 chemically competent cells	Invitrogen	C404004
TOPO XL PCR Cloning Kit	Invitrogen	45-0008LT
Envision ARK kit	DAKO	Cat#3954
XT index kit	Nextera	FC-131–1001
Experimental Models: Organisms/Strains		
Mouse: C57BL/6J-Apc^{Min}/J	Jackson Laboratories	stock no. 002020
Mouse: B6.Cg-Tg(UBC-cre/ERT2)1Ejb/1J	Jackson Laboratories	stock no. 007001
Mouse: (Gt(ROSA)26Sor$^{tm1(CAG-Brainbow2.1)Cle}$/J	Jackson Laboratories	stock no. 137331
Mouse: B6.Cg-Apc^{tm2Rak}/Nci	National Cancer Institute Mouse Repository	strain no. 01XAA
Mouse: MMTV-Myc [a.k.a., Tg(MMTV-Myc)141–3Led]	National Cancer Institute Mouse Repository	strain no. 01XG2 NCI, MMHCC
Mouse: MMTV-rtTA [a.k.a., MTB]	Chodosh Laboratory University of Pennsylvania	Gift
Mouse: TetO-Wnt1 [a.k.a., TWNT]	Chodosh Laboratory University of Pennsylvania	Gift
Oligonucleotides		
β-catenin PCR and Sanger Sequencing: 5'-GCGTGGACAATGGCTACT CAA	This Paper	N/A
β-catenin PCR and Sanger Sequencing: 5'-GCGTCAAACTGCGTGGA TGG	This Paper	N/A
rtTA PCR and Sanger Sequencing: 5'-GCCCAGAAGCTAGGTGTAG	This Paper	N/A
rtTA PCR and Sanger Sequencing: 5'-CGAATAAGAAGGCTGGCTCTGC	This Paper	N/A
Apc PCR and Sanger Sequencing: See STAR Methods	This Paper	N/A
Apc^{mmcr} High Throughput Sequencing: 5'-TCGTCGGCAGCGTCAGAT GTGTATAAGA GACAGACAGAAAGTACTCCAGACGGG	This Paper	N/A
Apc^{mmcr} High Throughput Sequencing: 5'-GTCTCGTGGGCTCGGAGA TGTGTATAAG AGACAGTGGCTTGGCGTGATGACTTTG	This Paper	N/A
Gapdh qRT-PCR probe	Applied Biosystems	435239E
Wnt1 qRT-PCR probe	Applied Biosystems	Mm_01300555_g1
Other		

REAGENT or RESOURCE Antibodies	SOURCE	IDENTIFIER
Growth Factor Reduced Matrigel Mix	BD Biosciences	Cat#356231
DRAQ5	Cell Signaling	4084S
Collagenase	Sigma	C9891
Hyaluronidase	Sigma	H3406
Dispase / Neutral Protease	Roche	0492078001